Sub-scale Orion Parachute Test Results From the National Full-Scale Aerodynamics Complex 80- by 120-ft Wind Tunnel

Brian P. Anderson[*], James S. Greathouse[†], Jessica M. Powell[†]
NASA Johnson Space Center, Houston, TX 77573, USA
James C. Ross[‡], Edward T. Schairer[§], Laura Kushner[¶], Barry J. Porter[‖]
NASA Ames Research Center, Moffett Field, CA 94035, USA
Patrick W. Goulding II[**]
National Full-Scale Aerodynamics Complex, National Aerospace Solutions, LLC, Moffett Field, CA 94035, USA
Matthew L. Zwicker[††], Catherine Mollmann[‡‡]
Airborne Systems North American, Pennsauken, NJ, 08109, USA

A two-week test campaign was conducted in the National Full-Scale Aerodynamics Complex 80x120-ft Wind Tunnel in support of Orion parachute pendulum mitigation activities. The test gathered static aerodynamic data using an instrumented, 3-tether system attached to the parachute vent in combination with an instrumented parachute riser. Dynamic data was also gathered by releasing the tether system and measuring canopy performance using photogrammetry. Several canopy configurations were tested and compared against the current Orion parachute design to understand changes in drag performance and aerodynamic stability. These configurations included canopies with varying levels and locations of geometric porosity as well as sails with increased levels of fullness. In total, 37 runs were completed for a total of 392 data points. Immediately after the end of the testing campaign a down-select decision was made based on preliminary data to support follow-on sub-scale air drop testing. A summary of a more rigorous analysis of the test data is also presented.

I. Introduction

The nominal Orion parachute system under development by the Capsule Parachute Assembly System (CPAS) team is composed of three mortar-deployed forward bay cover parachutes, two mortar-deployed drogue parachutes, three pilot parachutes, and three pilot-deployed main parachutes. The CPAS concept of operations for a nominal scenario is depicted in Figure 1.

[*]CPAS Deputy Project Manager, Project Management Branch, Mail Stop EA5-2, AIAA Member.
[†]Aerodynamic Engineer, Applied Aeroscience & CFD Branch, Mail Stop EG3
[‡]Aerospace Engineer, Experimental Aero-Physics Branch, Mail Stop 260-1, AIAA Associate Fellow.
[§]Aerospace Engineer, Experimental Aero-Physics Branch, Mail Stop 260-1
[¶]Instrumentation Engineer, Wind Tunnel Systems Branch, Mail Stop 227-1, AIAA member
[‖]Senior Engineer, Aerospace Computing, Inc., Mail Stop 260-1, AIAA Senior Member.
[**]Systems Safety Engineer / Master Certified Test Director, AIAA Member.
[††]Senior R&D Engineer, 5800 Magnolia Ave
[‡‡]Production Engineer, 5800 Magnolia Ave, AIAA Member.

During development efforts, several air drop tests were conducted to understand the effects of a failed main parachute. Through December 2014, five 2-main parachute tests of the Engineering Development Unit (EDU) parachutes had been completed. During four of the five air drop tests, a pendulum swinging motion was observed. This pendulum motion has the undesirable effect of increasing the rate of descent, introducing a horizontal component of velocity, and increasing the hang angle of the capsule at touchdown. After making these pendulum observations, CPAS provided the Orion Guidance, Navigation, and Control (GN&C) and structures groups with an empirical parachute model[1] based on the drop test data for assessment of the pendulum effects on vehicle control and the vehicle structure. These assessments showed an unacceptable risk to the spacecraft structure.[2] The Orion Program asked the CPAS team to investigate design changes to the main parachutes that could help mitigate the pendulous motion.

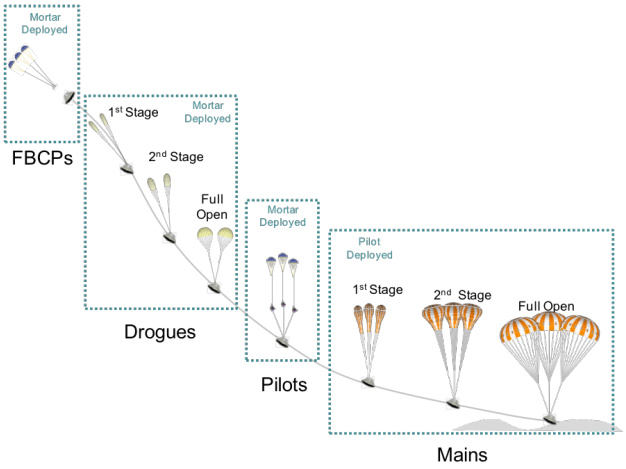

Figure 1: Nominal CPAS concept of operations.

A large effort by the Pendulum Action Team was carried out to understand the root cause of the pendulous motion. During this effort they considered many possible causes and their work included root cause diagrams, static aerodynamic analyses using rigid-body Computational Fluid Dynamics (CFD), dynamic aerodynamic extraction of the EDU parachutes from drop test data, wind assessments, and parachute-capsule motion reconstruction.[2] In the Pendulum Action Team's report, they noted:

1. Aerodynamically unstable main parachutes are the root-cause of the pendulum motion
2. Winds are a contributor, but the parachutes need to be unstable in order for the system to be in pendulum motion.

As a result of these findings, the CPAS team developed a plan to investigate changes to the main parachute design in an attempt to make the parachutes more aerodynamically stable. This plan consisted of application of historical knowledge, rigid-body CFD,[4] full-scale air drop testing, and sub-scale parachute testing. It should be noted that while Fluid Structure Interaction (FSI) computations would be an ideal tool for this study, the team felt that the available tools were not adequate to meet the stringent technical and schedule constraints. The sub-scale parachute testing included both wind tunnel (described in this paper) and air drop test campaigns.[3] In actuality, the pendulum mitigation efforts involved much more than the parachute designs in that the Orion Program also considered changes to GN&C designs as well as a number of structural assessments.[2] While not discussed in detail in this paper, a pictorial view of the work performed by the CPAS team as part of the pendulum mitigation activities is shown in Figure 2.

This paper documents the sub-scale wind tunnel test executed in the National Full-Scale Aerodynamics Complex (NFAC) 80x120-ft Wind Tunnel of 35% scale versions of the Orion main parachutes.

II. Test Overview and Objectives

The purpose of the test was to investigate aerodynamic stability and drag performance of various sub-scale main parachute canopy designs to inform the design of the full-scale parachute.

The objectives of this test were to:

1. Down select to two candidate canopy configurations for sub-scale air drop tests, and;

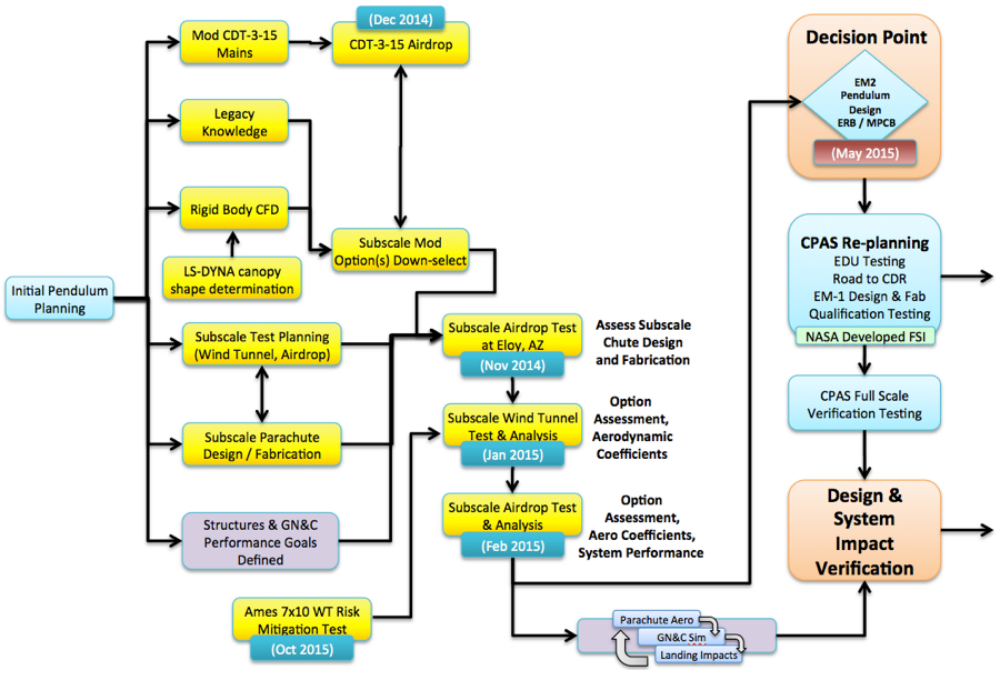

Figure 2: Pictorial view of the overall pendulum mitigation plans.

2. Gather single-canopy aerodynamic data for the selected parachute configurations to understand quantitative changes to canopy stability and drag performance.

Based on pre-test studies using CFD,[4] it was expected that blockage and wall-effects would affect the parachute motion and overall aerodynamics. In addition, the dynamic aerodynamic performance between the sub-scale testing and full-scale drop tests was expected to be different due to scaling. Because of these two considerations, drag performance and stability of each configuration were assessed relative to a scaled version of the Engineering Development Unit (EDU) parachute which has been used extensively during full-scale air drop tests.

Static aerodynamic performance was measured by instrumenting the parachute riser and each member of a 3-tether system attached to the parachute vent. The tether forces and riser loads were combined in a vector sum to determine the force required to restrain the parachute in various attitudes. These forces were converted to axial force and normal force coefficients (C_A and C_N).

Motion tracking using a series of photogrammetric images of the free-flying parachute was used to derive dynamic aerodynamic data. In addition, the qualitative assessments of each canopy's dynamic behavior was assessed by observing the parachute motion during the tests by eye.

III. Limitations and Assumptions

Sub-scale testing imposed a variety of physical and programmatic constraints and limitations on the test approach and design. Some of these led directly to planning compromises and necessitated assumptions to allow viable testing within the constraints at play. These considerations are summarized below:

Limitations

- The sub-scale test program was executed on an extremely aggressive schedule, with wind tunnel and

drop-test planning, data collection, and data reduction and analysis requiring completion within a 7-month window. This precluded the ability to thoroughly optimize the chosen scale of the test assets and greatly compressed the configuration down-select process moving from the wind tunnel to the drop-test phase.

- CFD predictions showed that significant blockage effects were expected at the chosen canopy scale in the wind tunnel. The ability to perform highly-accurate and reliable blockage corrections was limited.
- The wind tunnel support system rigidly fixes the canopy at the riser interface, which likely caused deviations in flight dynamics compared to free-flight.
- Blockage effects and physical size constraints precluded the ability to collect quality aerodynamic data on a cluster of two parachutes in the wind tunnel.

Assumptions

- The Pendulum Action Team concluded that aerodynamically-unstable main parachutes were a root-cause of the observed pendulum motion.[2] Thus it was assumed that if the canopy planform could be made more aerodynamically stable, the pendulum motion could be mitigated. This allowed the test team to pursue testing on single canopies in the wind tunnel to try to improve stability with reasonable levels of blockage.
- The test team assumed that gains in static stability would also improve dynamic stability, despite the lack of rigorous supporting data.
- The test team assumed that stability improvements in a single canopy would translate to similar improvements in the stability of a canopy cluster. This assumption could be corroborated by drop-testing cluster configurations following the wind tunnel test.
- The test team assumed that blockage and other tunnel effects acted similarly on all test configurations. This allowed valid conclusions to be drawn based on comparison between test configurations, despite the fact that the absolute data values were considered suspect.

IV. Parachute Model Descriptions and Candidate Configurations

The baseline (EDU) Orion parachute system is a ringsail parachute that includes 4 rings near the crown and 9 sails that extend from the rings to the skirt of the parachute. A 1.9% geometric porosity ring is included between sails 1 and 2. In addition to the resultant geometric porosity that comes as a result of the natural sail fullness, discrete geometric porosity "windows" are located at sail 7 in every fifth gore.

The CPAS team was tasked with identifying design changes that could improve the aerodynamic stability of the parachutes with the thought that this would, in turn, mitigate the pendulum motion per the findings of the Pendulum Action Team. In evaluating potential design changes, the team considered many factors including previous design updates to *Apollo* and *Orbiter*[5] parachutes that provided improved stability, CFD predictions,[4] and the experience and engineering judgment of parachute experts. The team was also careful to consider potential effects on the performance of the nominal 3-main parachute system, as the pendulum motion was only seen in a contingency 2-main parachute scenario, as well as ensuring that any design changes would not hinder the ability to apply the results of previous full-scale drop testing to evaluation of the final design. For example, drastically changing the porosity ring between sails 1 and 2, while potentially improving aerodynamic stability, could have impacts on parachute inflation and cluster behavior.

These considerations drove the team to consider three primary design trades: variation of geometric porosity in rings at sail 7, inclusion of "super sails" to bolster nominal fullness from 10% to 35% at sail 6, and effects of using an over-inflation control line (OICL). The super-sail configuration was meant to add porosity due to the increased sail fullness while also providing increased drag performance. OICLs have been used in the past to mitigate parachute breathing ("jelly-fishing") at the skirt with a minimal loss in drag. They differ from

reefing lines in that reefing lines drastically reduce the parachute skirt area. A geometric porosity ring near the skirt was predicted by static, rigid body CFD[4] to result in noticeable stability improvements with relatively small reductions in overall drag. Previous research and simulations suggested that these updates provided the best opportunity to leverage significant improvements in canopy stability with minimal compromise to overall drag performance.

The team settled upon a scale of 35% for the sub-scale test series as a compromise between tunnel blockage concerns and the need to ensure sufficient scale to adequately model representative construction and realistic dynamic behavior in flight. This resulted in a reference diameter of 40.8 ft and a rough weight of 30 lbm. The major design and construction parameters for the sub-scale canopies are summarized in Table 1.

Parameter	**Value**
Canopy scale	35%
Nominal diameter (D_o)	40.6 ft
Inflated diameter	28 ft
Number of gores	80
Number of rings	4
Number of sails	9
Construction material	1.1z Nylon broadcloth
Canopy mass	28.75 lbm
Trailing distance	58-ft
Suspension line ratio	$1.4D_o$

Table 1: Summary of sub-scale parachute design parameters

The schematics in Figure 3 show the three designs tested during the wind tunnel test campaign. All of them featured a 1.9% porosity ring between sails 1 and 2 to match the design of the baseline (EDU) asset. They featured variations in sail fullness and porosity near the canopy skirt, which CFD predicted could offer significant gains in stability with minimal effect on overall drag. All three configurations were tested both with and without an OICL.

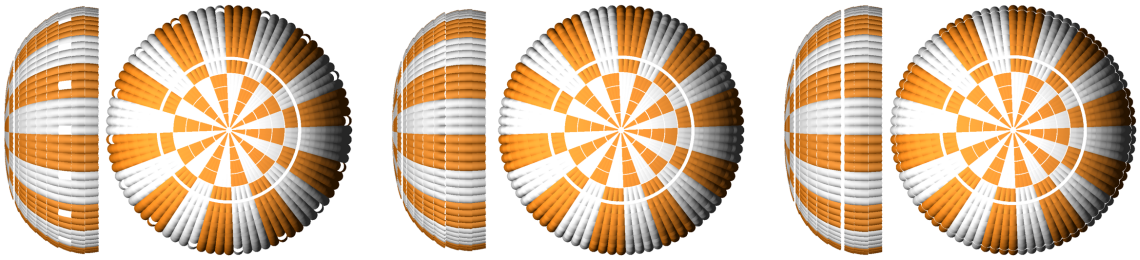

(a) Test Article 1, "EDU" (b) Test Article 2, "Super Sail" (c) Test Article 3, "Sail 7 Ring"

Figure 3: Sub-scale parachute test articles.

The first canopy design (Test Article 1), shown in Figure 3(a), represented the baseline or "EDU" design. This design featured the 1.9% porosity ring between sails 1 and 2 as well as discrete "windows" at every fifth gore on sail 7. This design allowed for direct comparison back to baseline drop test data obtained previously.

The second design (Test Article 2, Figure 3(b)) maintained the baseline 1.9% porosity ring between sails 1 and 2 but eliminated the porosity "windows" at sail 7. In lieu of this, the fullness of sail 6 was increased from the nominal 10% to 35%. This was done in the hopes of improving canopy drag performance with minimal compromise to stability. The baseline for this configuration did not include a geometric porosity ring at sail 7, but as the test progressed material was removed from sail 7 (cutting from the top of the sail down towards the skirt) to add a porosity ring.

The third and final design (Test Article 3, Figure 3(c)) included a 1.9% porosity ring between sails 1 and 2, "EDU fullness", and the addition of a 3% porosity ring at sail 7. As the test progressed the ring was increased by removing material from the top of sail 7. CFD results had predicted that this additional porosity could provide substantial stability improvements without significantly affecting drag performance.

V. Test Architecture

The wind tunnel test included a combination of standard tunnel support equipment with a variety of test-specific hardware and instrumentation. The sub-sections to follow will highlight the major test equipment. NFAC is run by a Combined Test Force through the US Air Force as part of Arnold Engineering Development Complex. The 80x120 is the largest wind tunnel in the world and features a closed-wall, open-circuit atmospheric test section measuring 80-ft in height and 120-ft in width. The test section features a model support system mounted on a turntable that measures 55 ft in diameter. The turntable can rotate 360 to simulate model yaw orientations and NFAC maintains a wide array of support struts used to install models at various heights in the wind tunnel. An array of six drive fans ? each 40-ft in diameter and powered by a 22,500 hp electric motor ? are located downstream of the test section and can provide test speeds from 0 to 100-kt. Models and large equipment are installed using two large model access doors which form the east wall of the test section. A 75-ton gantry crane allows equipment to be lifted in and out from the crane pad staging area just outside the wind tunnel. Smaller equipment can be installed using the freight elevator and either of two personnel access doors located on the west wall of the test section. These doors can also be opened in test to provide test section access and line of sight to the model at low test speeds.

A. Basic Test Equipment

Figure 4 shows the major test section equipment used in the CPAS test series in the 80x120. The test featured a single standard NFAC main strut and fairing assembly that raised the canopy attachment point to a height of 40 ft. The strut was mounted to the standard mount points on the NFAC model support system. Loads were measured using an in-line load cell, as will be described in the following section.

The test team designed and installed a test-specific tether system to restrain the canopy and study forces and behaviors with the canopy intentionally perturbed from a trimmed flight state. A previous test campaign in the 80x120[8] had attempted similar restraint of a canopy in flight using a single tether, which proved to be very difficult. After discussing the challenges encountered in this previous test campaign, the test team elected to improve the tether restraint system by shifting to a three-tether configuration, thus improving the capability to hold the canopy stable at high angles of attack (α). This allowed the test team to pull the canopy to fixed angles and measure the restorative forces driving it back toward a trim state using in-line load cells in the tether lines. The canopy could then be released from this perturbed position, allowing the team to study the re-trim behavior as it moved back into a trimmed state.

The test team used a short entry in the US Army's NASA Ames 7- by 10-foot Wind Tunnel as a proof of concept for the tether system functionality. This allowed the team to finalize the position and orientation of the tethers, verify the setup, and optimize procedures and operations at a more manageable scale. One tether was run through a pulley block attached near the center of the wind tunnel ceiling, and the other two were run through pulleys on rails mounted to the wind tunnel floor. The position of the ceiling pulley was

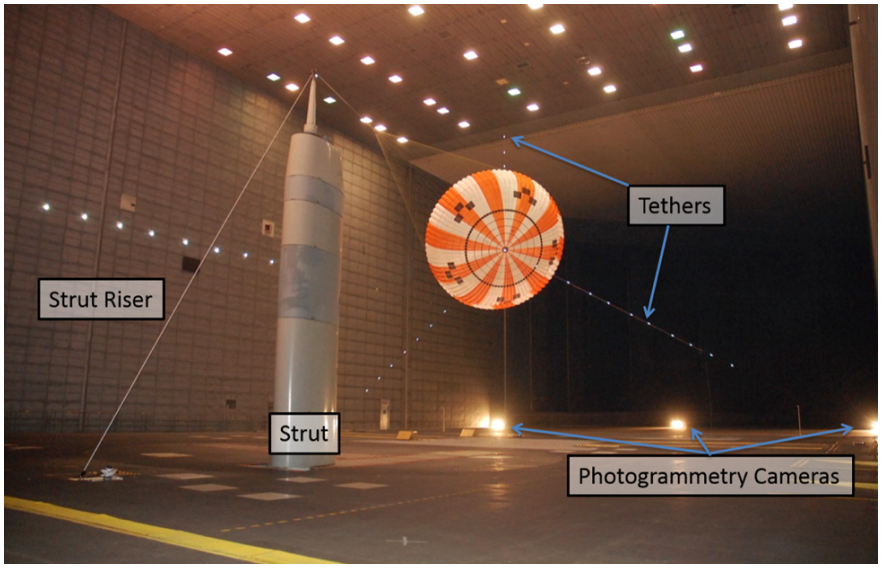

Figure 4: Overview of test equipment installed in the 80x120.

fixed at a location that allowed the best compromise through the desired α range, while the floor pulleys were installed on rails so that they could be repositioned as the canopy was yawed to maintain the tethers as near to tangential to the canopy apex as possible. The canopy α was adjusted using electric winches to remotely control the line length of each tether independently. By adjusting tether length, shifting the pulley block positions along the floor rails, and yawing the main strut on the turntable, the team was able to attain a wide range of canopy α settings. Restorative forces were measured using in-line load cells in each tether, as will be described in the following section.

The desired α range could not be attained by maintaining the strut in the center of the tunnel and pulling the apex of the canopy toward the wall. In order to increase the α range, the team had to yaw the turntable to skew the support strut to one side of the tunnel, while pulling the apex of the canopy to the opposite side, thus creating a larger total α. As the strut and the canopy moved along an arc, the relative distance between the canopy apex and the strut tip varied. This meant that this variation needed to be accommodated within the test setup. The team initially looked into installing a remotely controlled winch at the top of the strut to provide for this variation in length, but the logistic complications of this installation quickly made it untenable. The test team was able to devise a means of allowing this variation in a passive manner using a custom-designed strut tip.

The strut tip was designed with bearings and rollers that allowed for passive adjustment of the effective strut-riser support line length while keeping the end attached to a fixed position on the wind tunnel floor. The design of this strut tip is shown in Figure 5. The strut tip featured a large-diameter horizontal roller to turn the strut-riser line up and over the strut tip to a horizontal orientation where it attached to the parachute riser interface. The tip also included two sets of smaller-diameter vertical rollers to allow the tip to pivot with the canopy on a bushing fixed to the top of the strut. The fixed end of the strut riser line was attached to a cleat on the wind tunnel floor upstream of the support strut, routed through a block and pulley and up over the strut tip. The free end was attached to the parachute riser interface with an in-line load cell to measure canopy loads. As the strut and canopy were rotated through the α range, the strut-riser pushed against the rollers and caused the tip to rotate on its bearing. This caused the relative position between the strut-riser-to-riser interface and the strut tip to vary automatically, although the combined length of the strut-riser, riser, and suspension lines remained constant.

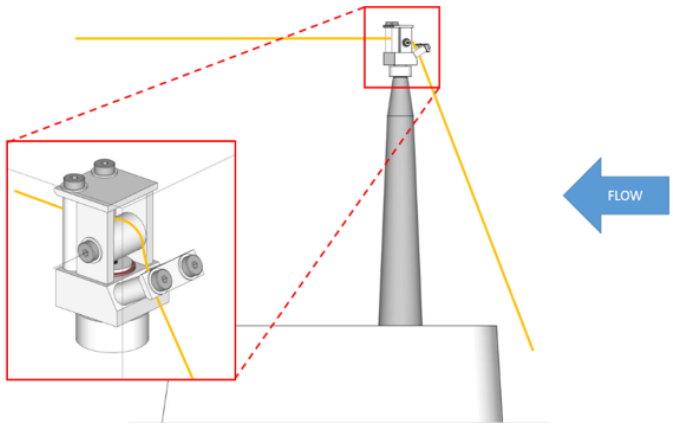

Figure 5: Detail of CPAS custom strut tip.

Rough α was set in test using visual markers on a monitor screen at the tether winch operator station. The precise α was computed using a series of cameras mounted downstream of the test section, performing stereo photogrammetry measurements on the position of the canopy apex.

B. Test Specific Instrumentation

Test-specific instrumentation included three primary categories: local dynamic pressure (Q) probes, the strut-riser load cell, and the tether line load cells. Photogrammetry equipment will be discussed in the following sub-section. Three local Q probes were installed in the test section. One was located upstream of the support strut and used to correlate with measured freestream Q. The other two were located approximately 20 feet downstream of the canopy apex, one on each side of the test section. All three were mounted to the test section floor. The average between the downstream probe responses was compared to the upstream probe response to obtain an estimate of Q augmentation due to canopy blockage. Due to the highly separated flow and recirculation expected in the canopy wake, it was assumed that the local Q downstream of the canopy would not be significantly different than the local Q abeam of the canopy. These data were used to assess blockage effects in the wind tunnel.

Canopy drag was measured using an S-type, in-line load cell installed between the free end of the strut-riser line and the canopy riser interface. The load cell had a 5000-lbf capacity and the instrumentation line was routed down the main strut and into the NFAC data system.

Each tether restraint line was also equipped with an in-line load cell to measure restorative forces and allow computation of C_N and C_A, which are used in the assessment of stability performance. These load cells had a 300-lbf capacity and were installed near the point at which the tethers connected to a common interface ring, which attached to the canopy apex. The instrumentation lines were physically bundled together and routed down one of the floor tether lines with sufficient service loop to allow adjustment of the tether length through the α range. These loads were also monitored in real-time to ensure the mounting hardware for the tether system did not experience excessive load.

C. Photogrammetry

A total of five cameras dedicated to photogrammetry were installed in the test section. Three of the cameras were used for canopy vent tracking in order to derive aerodynamic coefficients, while the other two cameras were used to gather information about canopy shape.

Each of the camera mounting brackets included lamps to illuminate targets on the canopy. An example of one of these brackets is shown in Figure 6. Calibration of the cameras was carried out using a similar method in previous NFAC testing[7] using a commercial photogrammetry system and calibration targets on the NFAC crane. The vent tracking cameras took data at 60Hz. Spatial accuracy for the canopy vent location was estimated at ±1-inch. The three cameras were synchronized with the wind tunnel data system using a simultaneous strobe within the camera view and a TTL pulse to the data system.

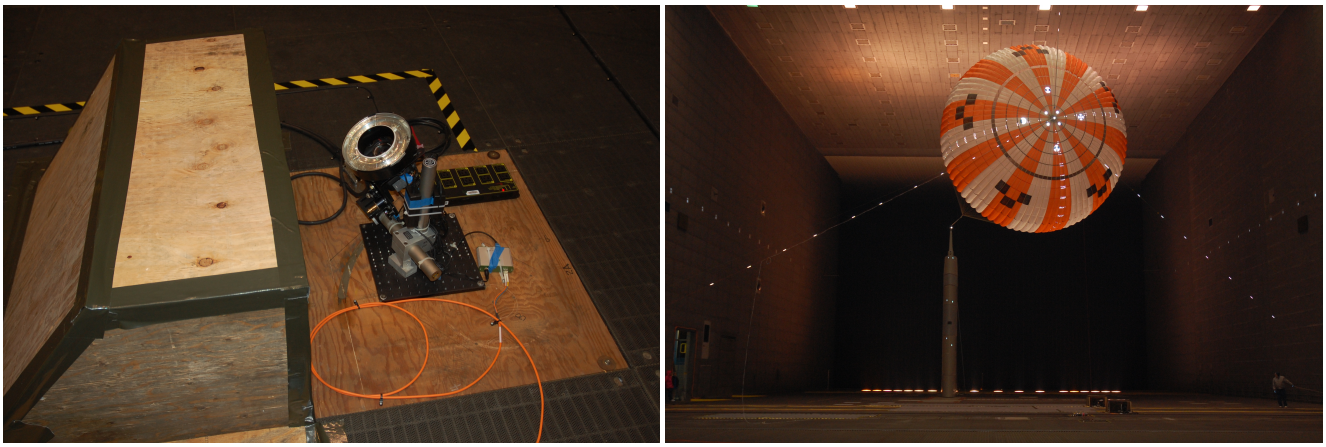

(a) Shape camera mounting station

(b) Retro-reflective target locations

Figure 6: Test hardware and features used in photogrammetry measurements

The three cameras used to track the canopy vent were placed in the constant area duct downstream of the 80x120 test section looking upstream at the canopy vent. To enable photogrammetry data collection a series of retro reflective targets were sewn onto the canopy near the vent. Retro-reflective targets were also placed on the vent tethers to determine the tether angles during the static runs to allow accurate vector summation of the tether and riser forces.

VI. Test Procedure and Matrix Summary

Over the course of the 10-day test entry, there were a total of 37 runs completed, comprising a total of 392 data points. Testing consisted of three major test techniques: static points, dynamic releases, and free flight. Data were obtained at various α and Q combinations on all three test canopies using each of these three basic test approaches. The details of these approaches are summarized below:

- Static test points were obtained by attaching the canopy apex to the tether system and using the tether to hold the canopy at a fixed α while data were collected. This was typically done for a series of α settings in a fixed αsweep schedule. This approach provided measurements of canopy drag along with restorative forces at fixed combinations of Q and α. Data were also acquired while transitioning between fixed α settings.
- Dynamic releases involved using the tether system to set a desired αat a given tunnel condition, then initiating a long-duration data point and releasing the canopy. Data were acquired from the strut-riser load cell as well as the photogrammetry systems to study the dynamic stability behavior of the canopy.
- Free flight points were generally acquired using long-duration data points with the canopy flying without obstruction. Similar data to the dynamic release points were acquired.

Generally, runs for a given test configuration consisted of attaching the canopy to the tether system, inflating

the canopy and setting the desired test speed, and sweeping the canopy through a set of α orientations while acquiring static points. Once all static data had been acquired, the canopy was released from the tethers during a dynamic release event and then one or more free flight points were acquired after the canopy had returned to a stable trim condition. The information in Table 2 summarizes the major data obtained on all three test articles.

Config.	**Test Article**	**Description**	**Static Data**	**Dynamic Release**	**Free Flight**
1	1	EDU w/ and w/o OICL	X	X	X
2	1	Reefed EDU (1st & 2nd stages)			X
3	2	Super sail, 1.6% porosity (w/ and w/o OICL)			X
4	2	Super sail, 2.3% porosity	X	X	
5	2	Super sail, 3% porosity (w/ and w/o OICL)	X	X	X
6	2	Reefed super sail, 3% porosity (1st & 2nd stages)			X
7	2	Super sail, 4% porosity	X	X	X
8	2	Super sail, 5% porosity	X	X	X
9	2	Super sail, 5.5% porosity	X	X	X
10	3	Slot, 3% porosity (w/ and w/o OICL)	X	X	X
11	3	Slot, 5% porosity	X	X	X
12	3	Reefed slot, 5% porosity (2nd stage only)			X
13	3	Slot with pleated skirt	X	X	
14	N/A	Dual canopies			X

Table 2: Test matrix summary

OICL length and other details were varied for each test article. The majority of the data were obtained at tunnel speeds of 16.5 and 20 kt, though free flight data were obtained at speeds from 7.5 to 30 kt. Select runs featured canopies equipped with reefing lines to simulate inflation shapes experienced by the parachutes in the first and second stages of their inflation cycles. These runs are designated in the descriptions in Table 2. Where not otherwise listed, all testing was conducted with the canopies in a full-open configuration. Testing at first and second stage conditions was completed at speeds from 30 to 45 kt. Data gathered with the pleated skirt and dual-canopy configurations were gathered as part of qualitative assessments of canopy shape and behavior.

VII. Initial Results and Canopy Down Select

The final testing was completed on Friday evening, but the down select decision was made earlier that same day. This decision was needed to allow Airborne Systems enough time to modify the remaining six sub-scale parachutes for use in the air drop testing 2-weeks later. This section presents the data that the down select decision was primarily based on. Section IX provides a summary of the test data analysis that was conducted after both the wind tunnel and air drop test campaigns were completed.

Any increase in porosity for the "slot" configuration (Figure 7) resulted in a noticeable reduction in axial coefficient as compared to the EDU configuration. In contrast, the super sail configuration (Test Article 2) with the same 3% geometry porosity ring had axial coefficient results very similar to the EDU parachute. It can also be seen that, as expected, the axial coefficient is reduced as the geometric porosity ring is enlarged. The normal coefficient plot in Figure 7 shows a measure of the parachute stability changes with canopy

configuration change. In general, and as expected, as the geometric porosity is increased, the magnitude of the normal coefficient was also increased.

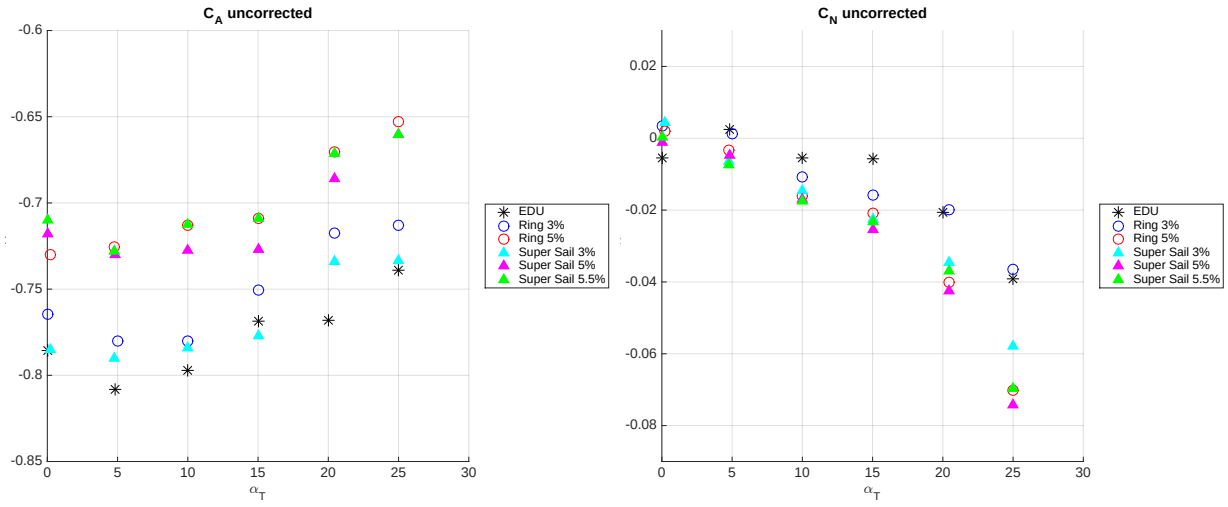

(a) Axial Force Coefficient

(b) Normal Force Coefficient

Figure 7: Quick look static data

Figure 8 shows a time history for the total angle of attack during dynamic runs for the EDU configuration as well as the super sail with 3% porosity and super sail with 5% porosity. This time history was derived from the vent tracking provided by photogrammetry. Both plots indicate that the total angle of attack range for both candidate configurations is smaller compared to the EDU configuration.

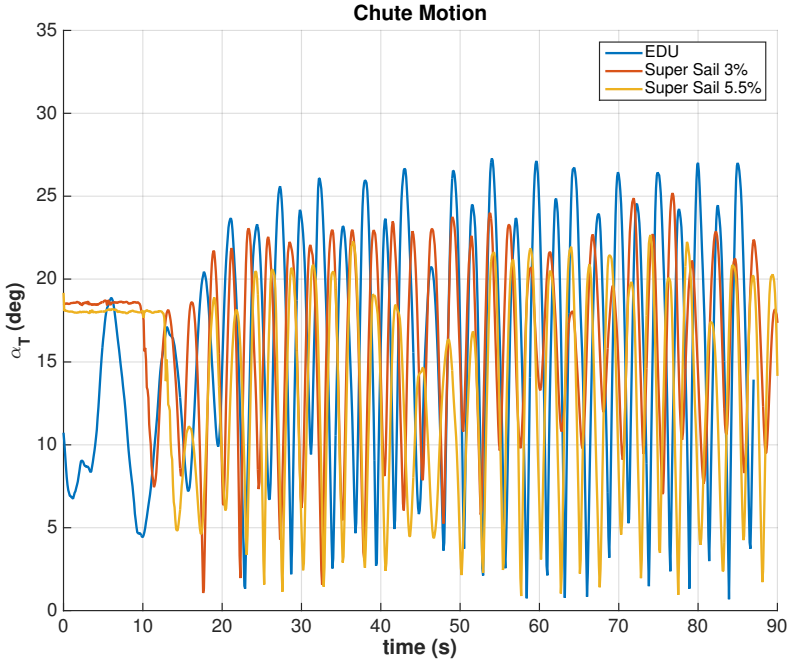

Figure 8: Total angle of attack time history

Based on both the static data presented in Figure 7 and the canopy motion information presented in Figure 8, the team decided that the super sail canopy with a 3% porosity ring and the super sail canopy with a 5.5% porosity ring should be selected for follow-on air drop testing. The super sail canopy with a 3% porosity ring was selected primarily because it showed the potential for increases in stability while maintaining the drag performance of the EDU canopy. The super sail canopy with a 5.5% porosity ring was selected due to its relatively small drag reduction with a substantial increase in static stability.

VIII. Data Reduction

This section contains some of the assumptions and information utilized in the more detailed analysis of the test data. Results of this more detailed analysis are shown in Section IX.

A. Time Syncing

The DAS and photogrammetry data were time synced by finding the peaks in the strobe firings from the DAS and attributing either the first or second peak to the strobe seen in one frame of the photogrammetry data. Then time zero is set by the first data point of whichever data source began recording second. The final data point is similarly set to the last data point of whichever data source stopped recording first. This means that the data was kept while there was data from both sources.

B. Blockage Correction

Previous testing of similarly sized parachutes in the NFAC 80x120 foot wind tunnel successfully made use of the Macha-Buffington blockage correction. It was shown that the data fit the Macha-Buffington correlation to within ±5%. However this previous testing was only done with essentially freeflight data, while this test looked at both freeflight and static data.

Figure 9 shows how the static and freeflight data for this test compare to the Macha-Buffington correlation. Despite some outliers the freeflight data mostly falls within the ±5% bounds, but the static data shows much higher differences between downstream and upstream dynamic pressure for a given drag value. This discrepancy may be due in part to the limitation of measuring downstream pressure with just a couple fixed probes.

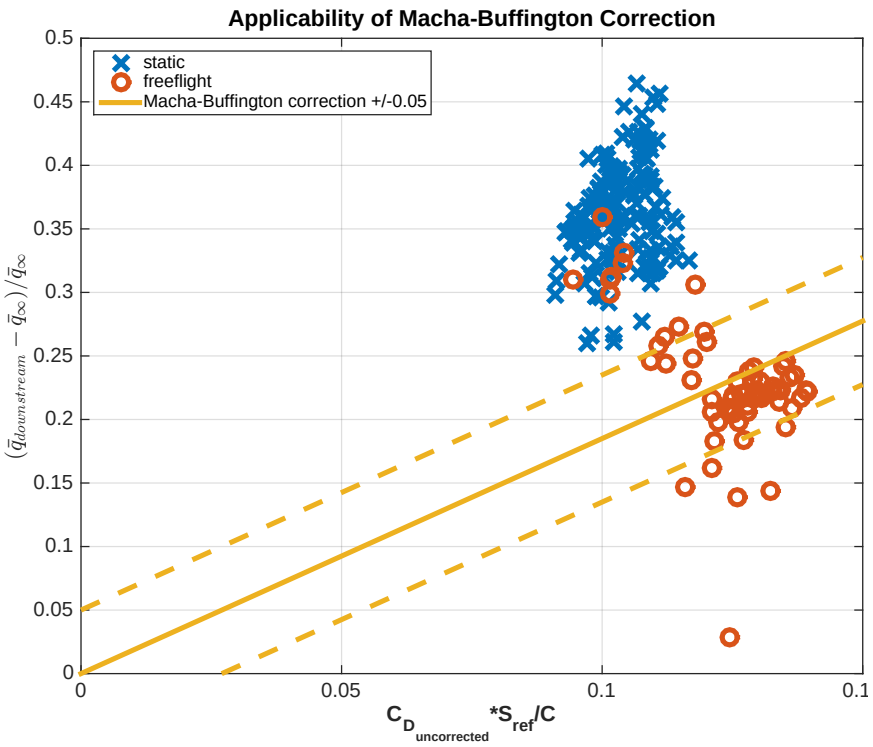

Figure 9: Comparison of Wind Tunnel Data to Macha-Buffington Correlation

Unfortunately, without more dynamic pressure measurements and without testing these canopies at a larger range of dynamic pressures, a better model for blockage correction cannot be directly determined. Even though these comparisons do not instill confidence in the applicability of the Macha-Buffington blockage correction to this data set (and particularly to the static data), some kind of correction is needed to reconcile the differences observed between static and freeflight drag. Figure 10 shows a comparison of static and freeflight axial force with and without this blockage correction for the EDU canopy. The freeflight points with the lowest axial force are most representative of the static values since dynamics results in drag augmentation. Clearly the blockage correction results in great agreement at the higher angles of attack. It is unlikely that there are truly static-like points at the lower angles of attack.

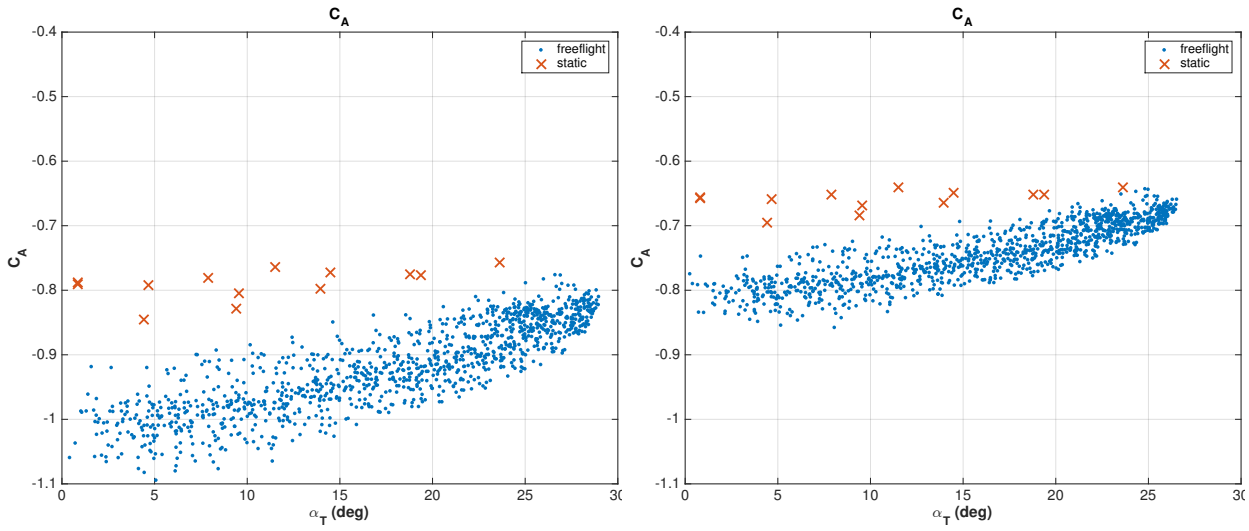

(a) No Blockage Correction

(b) With Blockage Correction

Figure 10: Effect of Blockage Correction

With the results of the static and freeflight axial force comparisons, it seems more reasonable to use the blockage correction. The corrected drag values are more in line with the expected drag of the canopy.

In the absence of additional evidence, it was decided to implement the blockage correction and accept that there could be considerable error in the magnitudes of the aerodynamic coefficients. Since the emphasis of this work was on comparing the aerodynamics of canopies rather than getting an exact measure of the aerodynamics of the individual canopies, the results should still be valid.

C. Apparent Mass

An assumed apparent mass was used for the initial processing. This definition is consistent with what is used in the aerodynamic modeling of the full scale third stage EDU parachutes. It treats the apparent mass as an approximation of the enclosed mass.

$$m = \frac{1}{2}\frac{4}{3}\pi\left(0.7\frac{l_{ref}}{2}\right)^3\rho$$

The center of mass of the parachute was assumed to be located at the center of the skirt.

IX. Results of Detailed Data Analysis

Following test completion, a fairly extensive review of the data was performed. This section contains select plots to explain the kinds of data available. There are additional plot sets (although not included in this paper) that capture the aerodynamics and parachute motion for each data point.

A. Parachute Motion

The overall stability of the parachutes can be assessed qualitatively by comparing the aerodynamic rates and peak vent amplitudes.

Figure 11 shows the trace of the vents of the three downselect configurations for dynamic and freeflight runs at 20kts. The dynamic cases begin oscillating horizontally, but eventually get into a vertical oscillation where the parachute exhibits severe shape changes near the peaks of the cycles. This is believed to be related to blockage and wall effects. For this reason the dynamic data, particularly the first couple cycles right after release, is likely the best data to analyze for dynamic aero.

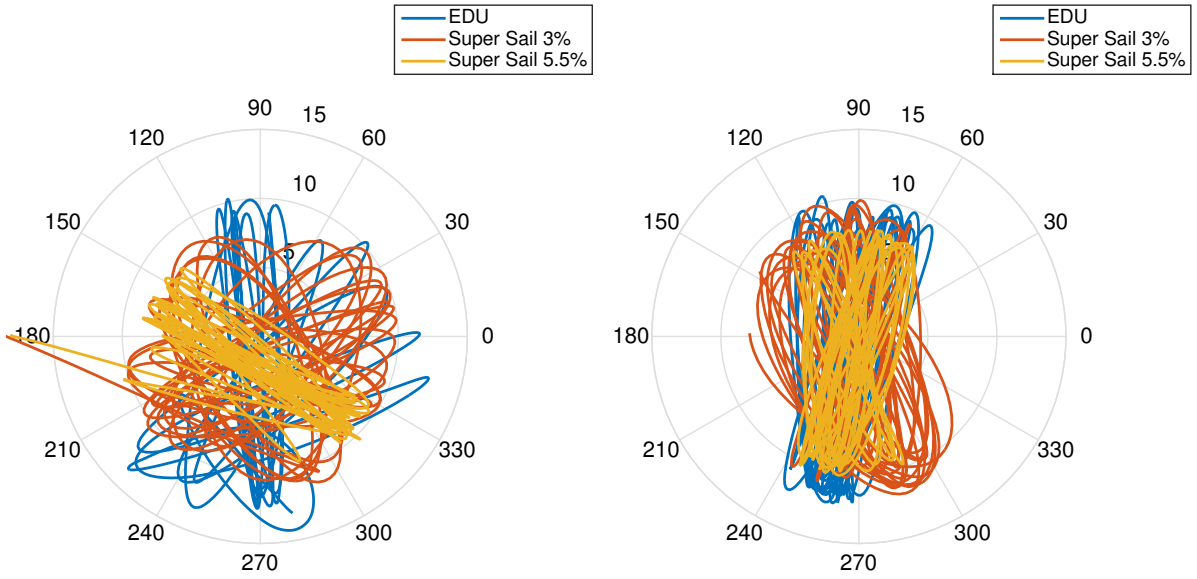

(a) Dynamic Comparison

(b) Freeflight Comparison

Figure 11: Vent Trace Polar Plots

Figure 11 also shows that the amplitude of the oscillations decrease with add porosity at the 0.8 location. This is an indication that the porosity is improving the aerodynamic stability of the parachutes.

B. Static Data

The static aero was computed as an average of usually ∼30 seconds (earlier data sets had only 500 frames of photogrammetry data) of time synced data.

Figure 12 shows the static aerodynamic results for the three downselect configurations. These trends are consistent with expectations and with the reconstructed aerodynamics from the drop testing. There is a clear trend of increased static stability with added porosity.

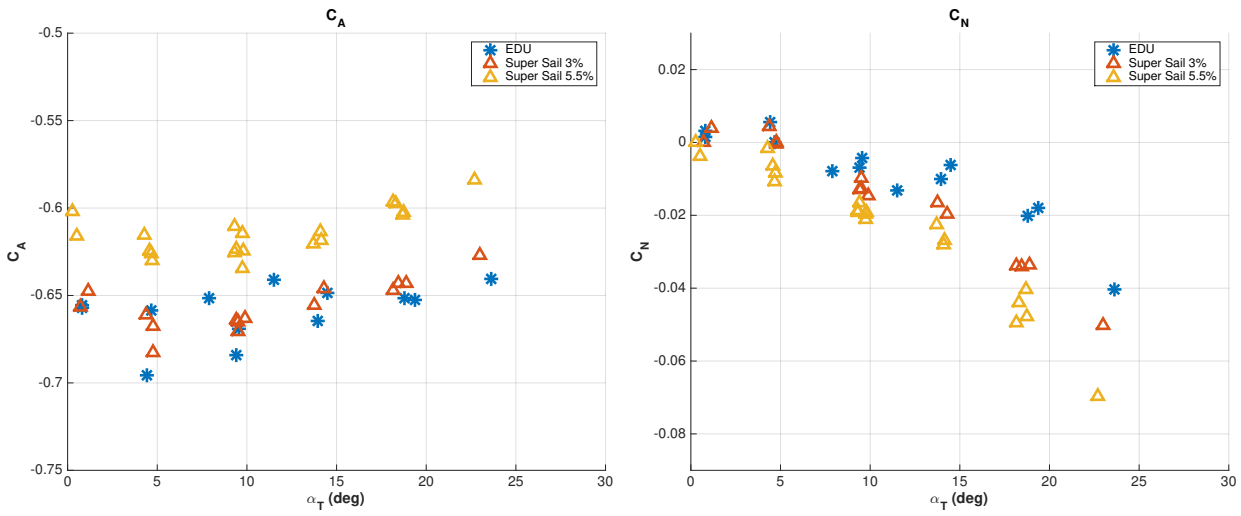

(a) Axial Force Coefficient

(b) Normal Force Coefficient

Figure 12: Static Aerodynamic Results

At low angles of attack all of the parachutes experienced fairly heavy breathing which resulted in significant variation in the aerodynamic coefficients. This means that the data cannot be used to determine the trim point. Figure 13 shows the static results for the EDU parachute. The bars show 1-sigma variation in the aerodynamic coefficients over time.

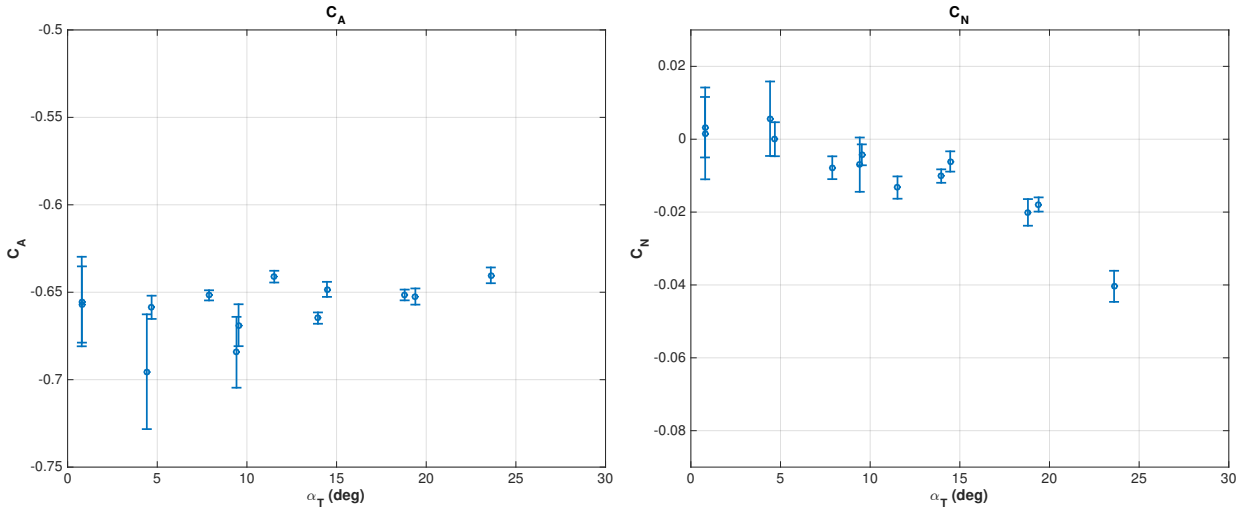

(a) Axial Force Coefficient

(b) Normal Force Coefficient

Figure 13: Impact of Breathing on Static Aero

C. Freeflight Data

In Section A the differences between the types of motion observed in dynamic and freeflight data was discussed. In many cases freeflight data points were taken directly after dynamic data points and there was sometimes residual dynamic-type motion in these freeflight points. It should also be noted again that some of the early data (freeflight data) was taken with the tunnel doors closed. The effect of this is unknown.

Figure 14 shows instantaneous axial and normal force coefficients computed for the Super Sail 5.5% configuration plotted against total angle of attack.

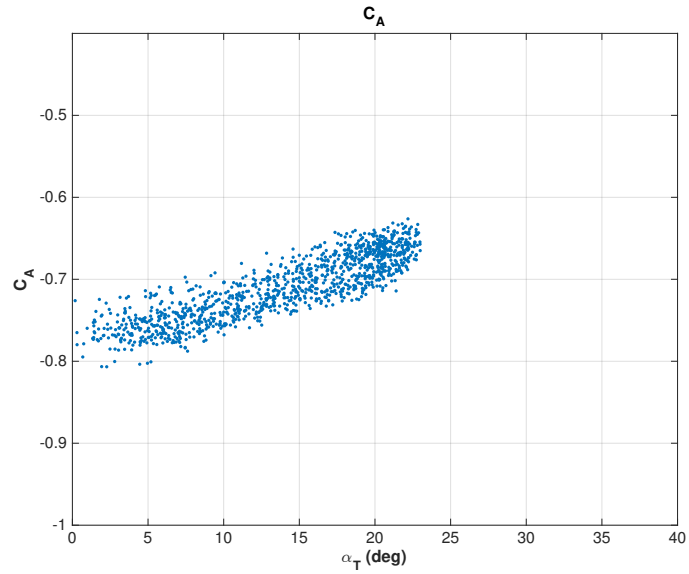

(a) Axial Force Coefficient

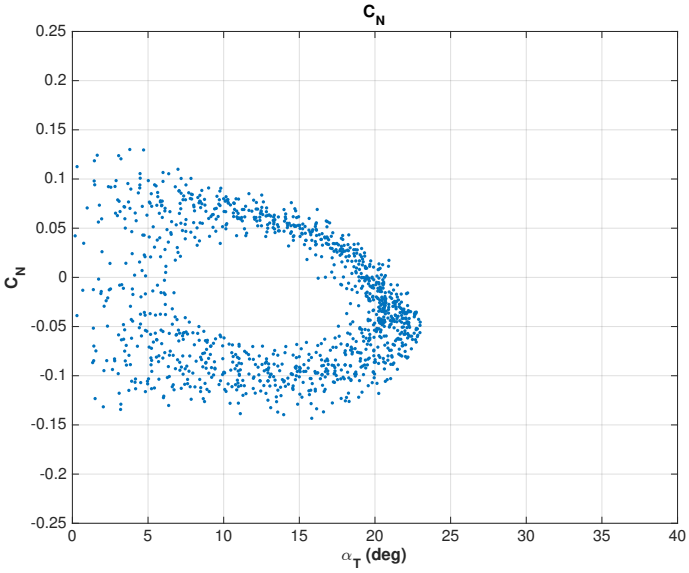

(b) Normal Force Coefficient

Figure 14: Freeflight Total Aero against Total Angle of Attack

Figure 15 shows the axial and normal force coefficients computed for the Super Sail 5.5% plotted against the rate of change of total angle of attack.

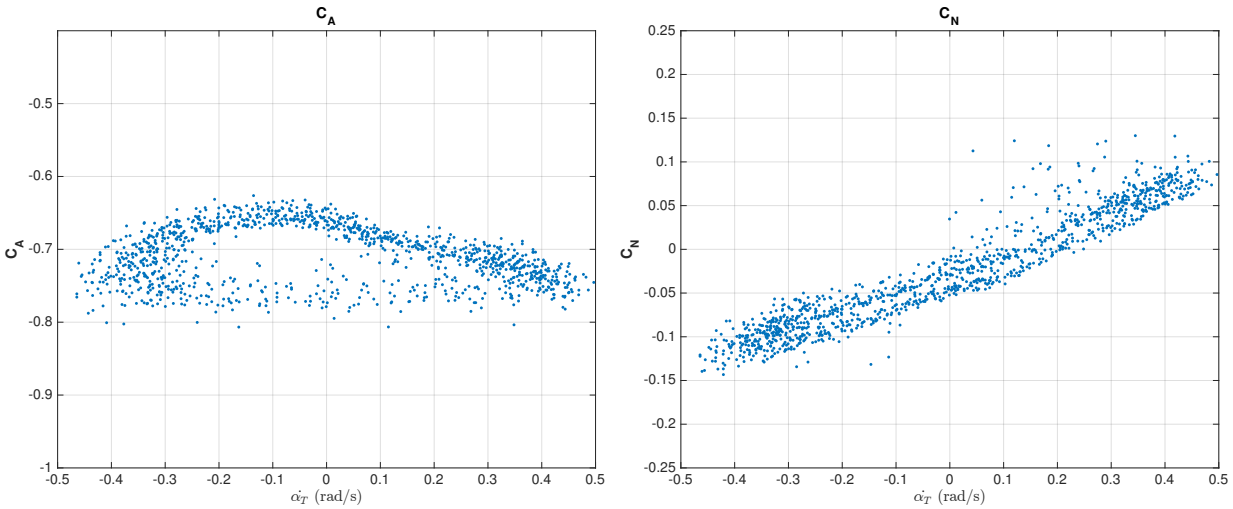

(a) Axial Force Coefficient

(b) Normal Force Coefficient

Figure 15: Freeflight Total Aero against Derivative of Total Angle of Attack

Figure 16 compares the axial and normal force coefficients of the three downselect configurations. While there is an obvious offset in the axial force due to the static contributions, the differences in the dynamic values appear to be relatively small. For the normal force, the dynamic values appear identical. While this only gives a rough sketch of the dynamic aero values, it does indicate that adding porosity at the 0.8 location does not impact the dynamic stability of the canopy.

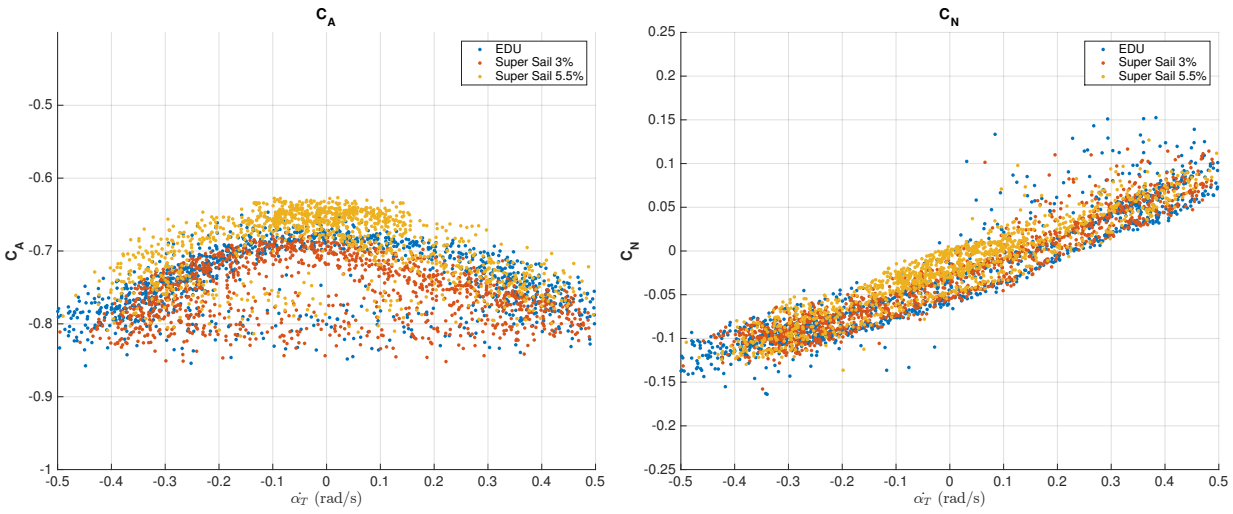

(a) Axial Force Coefficient

(b) Normal Force Coefficient

Figure 16: Freeflight Downselect Aero Comparisons

D. Dynamic Data

The dynamic data is essentially part static and part freeflight data. While the tethers are attached the data is processed like the static data points and once the tethers detach the data is processed like the freeflight data. The importance of the dynamic data is in the data just following release. The parachute is in a much more controlled motion and has angular rates that aren't observed at some angles of attack for the freeflight data.

Figure 17 compares the two dimensional independent parameter spaces of the dynamic freeflight data sets for the downselect configurations. The dynamic data sets do a good job of filling in the large central gap left in the freeflight parameter space.

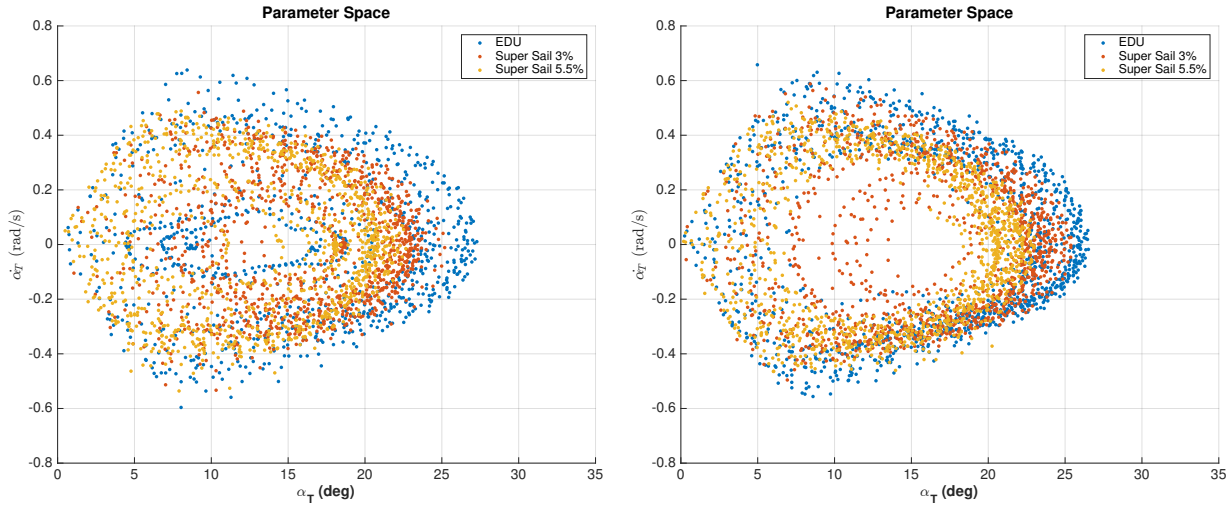

(a) Dynamic Data

(b) Freeflight Data

Figure 17: Data Parameter Space

Figure 18 shows the axial and normal force coefficients computed for the Supersail 5.5% configuration plotted against total angle of attack. The dots in blue are before the tethers were released and the orange are after the release. Comparing to Figure 14 it is again clear that the parameter space is better filled by the dynamic data.

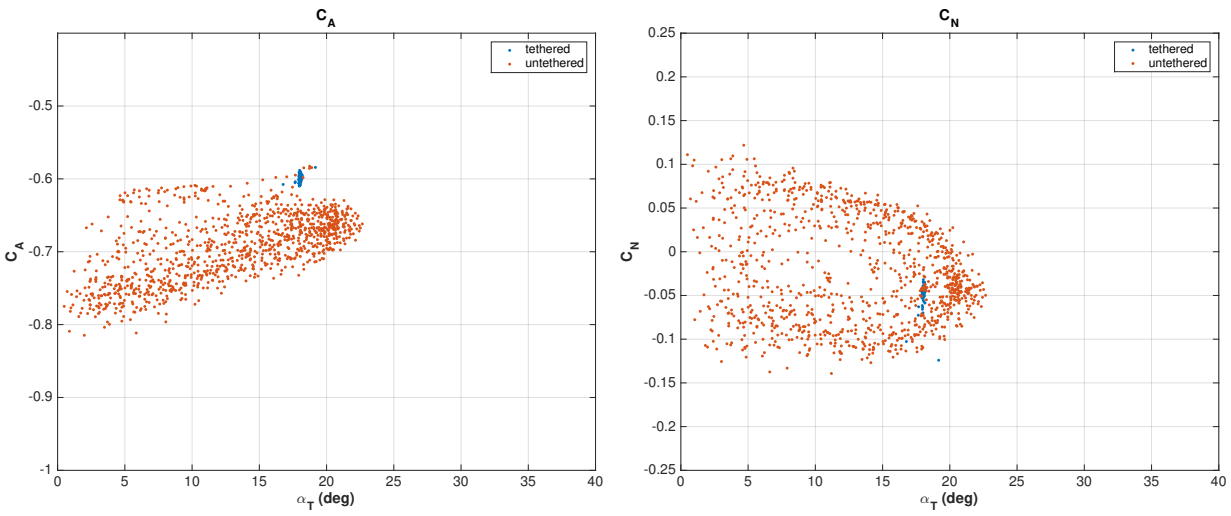

(a) Axial Force Coefficient

(b) Normal Force Coefficient

Figure 18: Dynamic Total Aero vs Total Alpha

X. Summary

A two-week test campaign was conducted in the National Full-Scale Aerodynamics Complex 80x120-ft Wind Tunnel in support of Orion parachute pendulum mitigation activities. In total, 37 runs were completed for a total of 392 data points. The test gathered static aerodynamic data using an instrumented 3-tether system attached to the parachute vent. Dynamic data were also gathered by releasing the canopy from a pre-determined orientation and measuring system performance using photogrammetry. Parachute configurations tested included a baseline canopy configuration based on the current Orion parachute design, a configuration with sails that had additional fullness and added geometric porosity, and a configuration with a geometric porosity slot near the skirt. At the end of the testing campaign a down-select decision was made based on the preliminary data to support follow-on sub-scale air drop testing. Following the test, a more rigorous data analysis was completed and this data has been presented in this paper.

XI. Acknowledgments

The authors thank the entire NFAC testing team who executed the testing extremely well, including a change-out of critical hardware in the weeks leading up to the test. The test team also thanks Ian Clark and Chris Tanner from the Jet Propulsion Laboratory for their guidance on the test techniques based on their experience during the LDSD program.

References

[1]Ray, Eric S., Machin, Ricardo A., *Pendulum Motion in Main Parachute Clusters*, 23rd Aerodynamic Decelerator Systems Conference, AIAA 2015-2138.

[2]Ali, Yasmin et. al., *Orion Multi-Purpose Crew Vehicle Solving and Mitigation the Two Main Cluster Pendulum Problem*, 24th Aerodynamic Decelerator Systems Technology Conference, Denver, Colorado, June 2017, submitted for publication.

[3]Daum, J. and Mollmann, C., *Design and Drop Testing of the Capsule Parachute Assembly System Sub-Scale Drop Main Parachute*, 24th Aerodynamic Decelerator Systems Technology Conference, Denver, Colorado, June 2017, submitted for publication.

[4]Greathouse, James S. and Schwing, Alan M., *Study of Geometric Porosity on Static Stability and Drag using Computational Fluid Dynamics for Rigid Parachute Shapes*, 23rd Aerodynamic Decelerator Systems Conference, AIAA 2015-2131.

[5]*Orbiter Drag Chute Stability Test in the NASA/Ames 80x120 Foot Wind Tunnel*, Sandia National Laboratories, SAND93-2544, Albuquerque, NM, February 1994.

[6]*Test Plan for the LDSD Subscale Parachute Testing at the NASA Ames Research Center National Full-Scale Aerodynamics Complex 80x120 Test Section*, Version 2.3, September 2012.

[7]Gonyea, K., Tanner, C., Clark, I., Kushner, L., Schairer, E., Braun, R., *Aerodynamic Stability and Performance of Next-Generation Parachutes for Mars Descent*, 22nd Aerodynamic Decelerator Systems Conference, AIAA 2013-1356.

[8]Tanner, C.L., Clark, I.G., Gallon, J.C., Rivellini, T.P., and Witkowski, A., ?Aerodynamic Characterization of New Parachute Configurations for Low-Density Deceleration,? AIAA Paper 2013-1358 presented at AIAA Aerodynamic Decelerator Systems Conference, Daytona Beach, FL, Mar. 25-28, 2013.